

# Theoretical investigation of the antimagnetic rotation in $^{104}\text{Pd}$ \*

Zhen-Hua Zhang <sup>1)</sup>

<sup>1</sup>Mathematics and Physics Department, North China Electric Power University, Beijing 102206, China

<sup>2</sup>Department of Physics and Astronomy, Mississippi State University, Mississippi 39762, USA

**Abstract:** The particle-number-conserving method based on the cranked shell model is used to investigate the antimagnetic rotation band in  $^{104}\text{Pd}$ . The experimental moments of inertia and reduced  $B(E2)$  transition probabilities are reproduced well. The  $J^{(2)}/B(E2)$  ratios are also discussed. The occupation probability of each orbital close to the Fermi surface and the contribution of each major shell to the total angular momentum alignment with rotational frequency are analyzed. The backbending mechanism of the ground state band in  $^{104}\text{Pd}$  is understood clearly and the configuration of the antimagnetic rotation after backbending is clarified. In addition, the crossing of a four quasiparticle states with this antimagnetic rotation band is also predicted. By examining the the closing of the four proton hole angular momenta towards the neutron angular momenta, the “two-shears-like” mechanism for this antimagnetic rotation is investigated and two stages of antimagnetic rotation in  $^{104}\text{Pd}$  are seen clearly.

**Key words:** particle-number conserving method, pairing correlations, antimagnetic rotation

**PACS:** 21.60.-n, 21.60.Cs, 23.20.Lv, 27.60.+j

## 1 Introduction

Antimagnetic rotation (AMR) [1, 2], which is predicted by Frauendorf in analogy to the antiferromagnetism in condensed matter physics, is an interesting exotic phenomena observed in some near spherical or weakly deformed nuclei. In AMR bands, higher angular momentum and energy are obtained by the “two-shears-like” mechanism, i.e., by simultaneously aligning of the angular momentum vector of two valence proton (neutron) holes toward that of the valence neutron (proton) particle. The AMR bands have regular sequences of energy levels differing in spin by  $2\hbar$ , which is the same as normal rotation. However, due to the weakly deformed or nearly spherical core, they are connected by weak  $E2$  transitions. Moreover, the  $B(E2)$  values decrease with increasing spin in AMR bands.

AMR has been investigated both experimentally and theoretically since it was proposed [2]. Up to now, evidence of AMR has been observed experimentally mainly in Cd ( $Z = 48$ ) and Pd ( $Z = 46$ ) isotopes including  $^{105}\text{Cd}$  [3],  $^{106}\text{Cd}$  [4],  $^{107}\text{Cd}$  [5],  $^{108}\text{Cd}$  [6, 7],  $^{110}\text{Cd}$  [8],  $^{101}\text{Pd}$  [9–11], and  $^{104}\text{Pd}$  [12]. Recently, possible AMR bands have also been reported in Eu ( $Z = 63$ ) isotopes including  $^{143}\text{Eu}$  [13] and  $^{142}\text{Eu}$  [14]. The existence of AMR still needs further investigation in  $^{109}\text{Cd}$  [15],  $^{100}\text{Pd}$  [16],  $^{144}\text{Dy}$  [17], and  $^{112}\text{In}$  [18] by lifetime measurements. AMR has been investigated theoretically mainly by the semi-classical particle rotor model [19], and the tilted

axis cranking (TAC) model [20–22]. Especially, many investigations have been performed within the framework of microscopic-macroscopic model [4, 6, 16], pairing plus quadrupole model [2, 15], and the covariant density functional theory (CDFT) [23–26] based on the TAC model (for reviews please see Refs. [27, 28]).

In Ref. [12], the ground state band (gsb) of  $^{104}\text{Pd}$  after backbending is assigned as AMR. Using the semi-classical particle rotor model, its configuration was assumed to be  $\pi g_{9/2}^{-2} \otimes \nu[h_{11/2}^2, (g_{7/2}, d_{5/2})^2]$  [12]. However, this band was assigned a different configuration as  $\pi g_{9/2}^{-4} \otimes \nu[h_{11/2}^2, (g_{7/2}, d_{5/2})^6]$  in a recent investigation using TAC-CDFT [26] with the point coupling effective interaction PC-PK1 [29]. Note that these two configurations are all written with respect to the  $^{100}\text{Sn}$  core. It can be seen that these two configuration assignments have different number of proton  $g_{9/2}$  holes, which are very important to the formation of AMR. Therefore, it is necessary to clarify the AMR configuration in  $^{104}\text{Pd}$ . In the present work, the particle-number-conserving (PNC) method [30, 31] based on the cranked shell model (CSM) will be used to investigate the AMR in  $^{104}\text{Pd}$ . Note that the PNC-CSM has already provided successful descriptions for the AMR bands in  $^{105,106}\text{Cd}$  [32] and  $^{101}\text{Pd}$  [33], and have shown the important role of pairing correlations on the moment of inertia (MOI) and the “two-shears-like” mechanism.

Different from the traditional Bardeen-Cooper-Schrieffer or Hartree-Fock-Bogoliubov approaches, in the

\* Supported by National Natural Science Foundation of China (11875027, 11505058, 11775112, 11775026, 11775099), Fundamental Research Funds for the Central Universities (2018MS058) and the program of China Scholarships Council (No. 201850735020)

1) E-mail: zhzhang@ncepu.edu.cn

PNC method, the pairing interaction is diagonalized directly in a sufficiently large Fock-space [34]. Therefore, it is a shell-model like approach and the particle-number is totally conserved from beginning to the end and the Pauli blocking effects are treated exactly. The PNC scheme has also been transplanted in relativistic and non-relativistic mean field models [35–38], and the total-Routhian-surface method [39].

This paper is organized as follows. The theoretical framework of PNC-CSM is presented in Sec. 2. The results and discussion of the AMR band in  $^{104}\text{Pd}$  are given in Sec. 3. Finally I summarize this work in Sec. 4.

## 2 Theoretical framework

For an axially deformed nucleus, the cranked shell model Hamiltonian reads

$$H_{\text{CSM}} = H_0 + H_{\text{P}} = H_{\text{Nil}} - \omega J_x + H_{\text{P}} , \quad (1)$$

where  $H_{\text{Nil}}$  is the Nilsson Hamiltonian [40],  $-\omega J_x$  is the Coriolis interaction, and  $H_{\text{P}}$  is the monopole pairing interaction with effective pairing strength  $G$ .  $H_{\text{P}}$  reads

$$H_{\text{P}} = -G \sum_{\xi\eta} a_{\xi}^{\dagger} a_{\bar{\xi}}^{\dagger} a_{\bar{\eta}} a_{\eta} , \quad (2)$$

where  $\bar{\xi}$  ( $\bar{\eta}$ ) denotes the time-reversal state of  $\xi$  ( $\eta$ ).

When treating the pairing correlations, a cranked many-particle configuration (CMPC) truncation is adopted, which can make sure that the PNC calculations are both workable and sufficiently accurate [34, 41]. For the investigation of heavy nuclei, a dimension of 1000 for both protons and neutrons is enough. By diagonalizing the  $H_{\text{CSM}}$  in a sufficiently large CMPC space, sufficiently accurate solutions for low-lying excited eigenstates of  $H_{\text{CSM}}$  can be obtained, which can be written as

$$|\Psi\rangle = \sum_i C_i |i\rangle , \quad (C_i \text{ is real}), \quad (3)$$

where  $|i\rangle$  is a CMPC (the eigenstate of  $H_0$ ) and  $C_i$  is the corresponding expanding coefficient. The expectation value of any one-body operator (e.g., angular momentum  $J_x$  and quadrupole moment  $Q_{20}$ )  $\mathcal{O} = \sum_{k=1}^N \mathcal{O}(k)$  can be written as

$$\langle \Psi | \mathcal{O} | \Psi \rangle = \sum_i C_i^2 \langle i | \mathcal{O} | i \rangle + 2 \sum_{i < j} C_i C_j \langle i | \mathcal{O} | j \rangle . \quad (4)$$

Since  $\mathcal{O}$  is a one-body operator, the matrix element  $\langle i | \mathcal{O} | j \rangle$  between two different CMPCs  $|i\rangle$  and  $|j\rangle$  is nonzero only when these two CMPCs differ by one particle occupation [31]. After certain permutations of creation operators, these two CMPCs can be written as

$$|i\rangle = (-1)^{M_{i\mu}} |\mu \dots \rangle , \quad |j\rangle = (-1)^{M_{j\nu}} |\nu \dots \rangle , \quad (5)$$

where  $\mu$  and  $\nu$  are two different single-particle states, and  $(-1)^{M_{i\mu}} = \pm 1$ ,  $(-1)^{M_{j\nu}} = \pm 1$  according to whether the number of permutation is even or odd. Therefore, the expectation value of the one-body operator  $\mathcal{O}$  can be separated into the diagonal  $\sum_{\mu} \mathcal{O}(\mu)$  and the off-diagonal  $2 \sum_{\mu < \nu} \mathcal{O}(\mu\nu)$  parts

$$\langle \Psi | \mathcal{O} | \Psi \rangle = \left( \sum_{\mu} \mathcal{O}(\mu) + 2 \sum_{\mu < \nu} \mathcal{O}(\mu\nu) \right) , \quad (6)$$

$$\mathcal{O}(\mu) = \langle \mu | \mathcal{O} | \mu \rangle n_{\mu} , \quad (7)$$

$$\mathcal{O}(\mu\nu) = \langle \mu | \mathcal{O} | \nu \rangle \sum_{i < j} (-1)^{M_{i\mu} + M_{j\nu}} C_i C_j , \quad (8)$$

where  $n_{\mu} = \sum_i |C_i|^2 P_{i\mu}$  is the occupation probability of the single-particle state  $|\mu\rangle$  and  $P_{i\mu} = 0$  (1) if  $|\mu\rangle$  is empty (occupied) in  $|i\rangle$ .

The kinematic MOI  $J^{(1)}$  and dynamic MOI  $J^{(2)}$  are given by

$$J^{(1)} = \frac{1}{\omega} \langle \Psi | J_x | \Psi \rangle , \quad J^{(2)} = \frac{d}{d\omega} \langle \Psi | J_x | \Psi \rangle . \quad (9)$$

The reduced  $B(E2)$  transition probability can be obtained from the semi-classical approximation as

$$B(E2) = \frac{3}{8} \langle \Psi | Q_{20}^{\text{P}} | \Psi \rangle^2 , \quad (10)$$

where  $Q_{20}^{\text{P}}$  is the proton quadrupole moment and

$$Q_{20} = \sqrt{\frac{5}{16\pi}} (3z^2 - r^2) = r^2 Y_{20} . \quad (11)$$

## 3 Results and discussion

In the present work, Nilsson parameters ( $\kappa$  and  $\mu$ ) for  $^{104}\text{Pd}$  are taken from Ref. [42]. The deformation parameter  $\varepsilon_2 = 0.18$  is taken as the experimental value [12]. The valence single-particle space is constructed from  $N = 0$  to  $N = 5$  major shells both for protons and neutrons. Note that  $N = 0$  to  $N = 3$  major shells are closed shells ( $N = Z = 40$ ), and are fully occupied, so their contribution to the total angular momentum alignment is zero both for protons and neutrons. However, they are important for calculating the  $B(E2)$  values. With  $N = 0$  to  $N = 3$  major shells being considered, there is no effective charge involved when calculating the  $B(E2)$  values. The effective monopole pairing strengths are determined by the experimental odd-even binding energy differences and the MOIs, and are connected with the dimension of the truncated CMPC space, which are about  $0.9\hbar\omega_0$  for protons and  $0.8\hbar\omega_0$  for neutrons, respectively. In the present calculations, the dimensions of the CMPC space are chosen as 1000 both for protons and neutrons, in which the CMPCs with weights larger than 0.1% in the many-body wave-function (c.f., Eq. 3) are all included.

The effective pairing strengths adopted in this work are  $G_p = 0.5$  MeV for protons and  $G_n = 0.8$  MeV for neutrons.

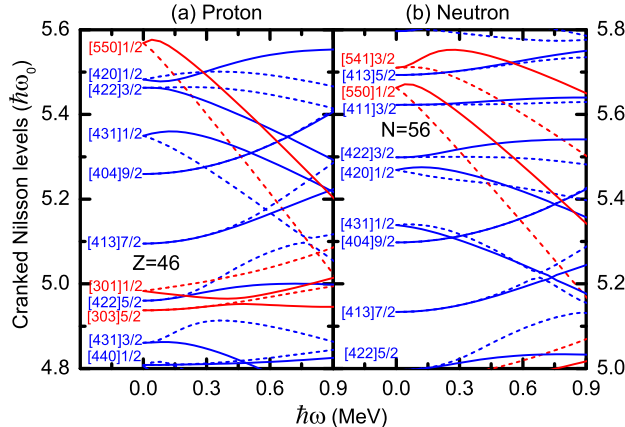


Fig. 1. (Color online) The proton (a) and neutron (b) cranked Nilsson levels near the Fermi surface of  $^{104}\text{Pd}$ . The positive and negative parity levels are denoted by blue and red lines, respectively. The signature  $\alpha = \pm 1/2$  levels are denoted by solid and dotted lines, respectively.

The cranked Nilsson levels near the Fermi surface of  $^{104}\text{Pd}$  are shown in Fig. 1 for (a) protons and (b) neutrons. Due to deformation effects, the traditional magic shell gaps with proton number  $Z = 50$  and neutron number  $N = 50$  disappear. It should be noted that since the quadrupole deformation adopted in the present calculation for  $^{104}\text{Pd}$  ( $\varepsilon_2 = 0.18$ ) is much larger than those for  $^{105}\text{Cd}$  ( $\varepsilon_2 = 0.12$ ),  $^{106}\text{Cd}$  ( $\varepsilon_2 = 0.14$ ), and  $^{101}\text{Pd}$  ( $\varepsilon_2 = 0.125$ ) in our previous works [32, 33], their single particle structures close to the Fermi surface are quite different. It can be seen from Fig. 1(a) that for the gsb of  $^{104}\text{Pd}$ , there are four  $g_{9/2}$  proton holes ( $\pi 9/2^+[404]$  and  $\pi 7/2^+[413]$ ). At rotational frequency  $\hbar\omega = 0$  MeV, they should be partly occupied due to the pairing correlations, and their occupation probabilities will change with increasing rotational frequency. Meanwhile, it can also be seen from Fig. 1(b) that the neutron  $h_{11/2}$  orbital  $\nu 1/2^-[550]$  should be nearly empty at rotational frequency  $\hbar\omega = 0$  MeV and with rotational frequency increasing, the single particle energy of this orbital decreases quickly. Different from the AMR band in  $^{101}\text{Pd}$  [9–11], the  $\nu 1/2^-[550]$  orbital is not blocked in the gsb of  $^{104}\text{Pd}$ , so neutron level crossing will happen with increasing rotational frequency. The data show that the possible AMR band in  $^{104}\text{Pd}$  is the yrast band after the backbending [12]. Using the semiclassical particle rotor model, its configuration was assumed to be  $\pi g_{9/2}^- \otimes \nu [h_{11/2}^2, (g_{7/2}, d_{5/2})^2]$  [12]. However, this band was assigned a different configuration as  $\pi g_{9/2}^- \otimes \nu [h_{11/2}^2, (g_{7/2}, d_{5/2})^6]$  in a recent investigation using TAC-CDFDT [26]. Therefore, to clarify its configuration,

in the following investigation, adiabatic calculations for the gsb in  $^{104}\text{Pd}$  will be performed and the configuration for this AMR band can be obtained automatically after neutron level crossings.

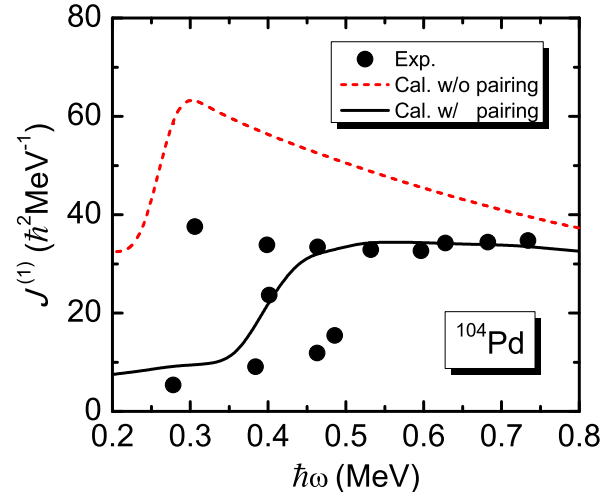


Fig. 2. (Color online) The experimental [12] and calculated kinematic MOIs  $J^{(1)}$  with and without pairing correlations for the gsb in  $^{104}\text{Pd}$ .

Figure 2 shows the experimental [12] and calculated kinematic MOIs  $J^{(1)}$  with and without pairing correlations for the gsb in  $^{104}\text{Pd}$ . The MOIs and the corresponding rotational frequencies are extracted by

$$\begin{aligned} \frac{J^{(1)}(I)}{\hbar^2} &= \frac{2I+1}{E_\gamma(I+1 \rightarrow I-1)}, \\ \hbar\omega(I) &= \frac{E_\gamma(I+1 \rightarrow I-1)}{I_x(I+1) - I_x(I-1)}, \end{aligned} \quad (12)$$

where  $I_x(I) = \sqrt{(I+1/2)^2 - K^2}$ . The pairing correlations are crucial to reproduce the data for the whole rotational frequency region. One can see from Fig. 2 that without pairing correlations, the MOIs of  $^{104}\text{Pd}$  are overestimated for a large extent and the calculated backbending frequency is much earlier than the data ( $\hbar\omega \sim 0.4$  MeV). After considering the pairing correlations, the data can be reproduced very well. Note that the present calculations fail to reproduce the sharp backbending appeared in the experimental MOIs due to the defect of the cranking model. In order to obtain the backbending effect exactly, one has to go beyond the cranking model [43, 44]. Due to the fact that the MOIs of the gsb in  $^{104}\text{Pd}$  are reproduced very well by the present PNC-CSM calculation, the configuration of this AMR band should be reasonable. Later on, the configuration obtained by the present calculation will be compared with previous works [12, 26].

Usually, typical AMR has weak  $E2$  transitions and large  $J^{(2)}/B(E2)$  ratios, which reflect the nearly spherical or weakly deformed core. Moreover, due to the

“two-shears-like” mechanism, the  $B(E2)$  values decrease with increasing spin. Figure 3(a) shows the experimental [12] and calculated  $B(E2)$  values with and without pairing correlations for the gsb in  $^{104}\text{Pd}$ . Previous works have shown that pairing correlations are important to reproduce the  $B(E2)$  values only when the proton level crossing happens, and the reduced  $B(E2)$  values strongly depend on the deformation rather than the superfluidity [32, 33]. It can be seen from Fig. 3 that the decreasing of the  $B(E2)$  values with increasing rotational frequency can be obtained no matter whether the pairing correlations are taken into account or not. However, the calculated results are more consistent with the data after considering the pairing correlations. Note that the experimental  $B(E2)$  values drop very quickly with increasing rotational frequency when  $\hbar\omega > 0.6$  MeV and the present calculation with fixed deformation fails to reproduce this. Therefore, the “two-shears-like” mechanism alone is not enough to provide the decrease of  $B(E2)$  values. The PNC-CSM calculations with deformation  $\varepsilon_2$  changing from 0.18 to zero are also shown in Fig. 3(a) by the blue dash dotted line. The inset shows the deformation parameter  $\varepsilon_2$  adopted in this calculation, which is obtained by fitting the experimental  $B(E2)$  values with increasing rotational frequency. It can be seen that at lower rotational frequency region, the deformation keeps nearly unchanged. With rotational frequency increasing, the deformation decreases gradually. When the rotational frequency  $\hbar\omega > 0.65$  MeV, the deformation shows a sharp reduction and decrease to zero rapidly at  $\hbar\omega \sim 0.75$  MeV. Due to the fact that with the experimental deformation parameter  $\varepsilon_2 = 0.18$ , the  $B(E2)$  values can be reproduced quite well at the beginning of this AMR band, the involution of the deformation with rotational frequency should be reasonable. Therefore, the present calculations also imply the quick reduction of the deformation in the gsb of  $^{104}\text{Pd}$  with increasing rotational frequency. Note that the TAC-CDFT calculations in Ref. [26], which can treat the deformation self-consistently with rotational frequency, can not reproduce such quickly decreasing  $B(E2)$  values neither. This may need further investigation. Figure 3(b) shows the comparison of experimental and calculated  $J^{(2)}/B(E2)$  ratios. Because the  $B(E2)$  values at higher spin region are not reproduced well by the PNC-CSM calculation with fixed deformation, only the first two data of  $J^{(2)}/B(E2)$  ratios can be reproduced reasonable well. It also can be seen that if the deformation changing effects are taken into account, the  $J^{(2)}/B(E2)$  ratios can be well reproduced, which is shown by the blue dash dotted line in Fig. 3(b). In addition, The sharp peak at  $\hbar\omega \sim 0.45$  MeV for  $J^{(2)}/B(E2)$  ratios is due to the backbending.

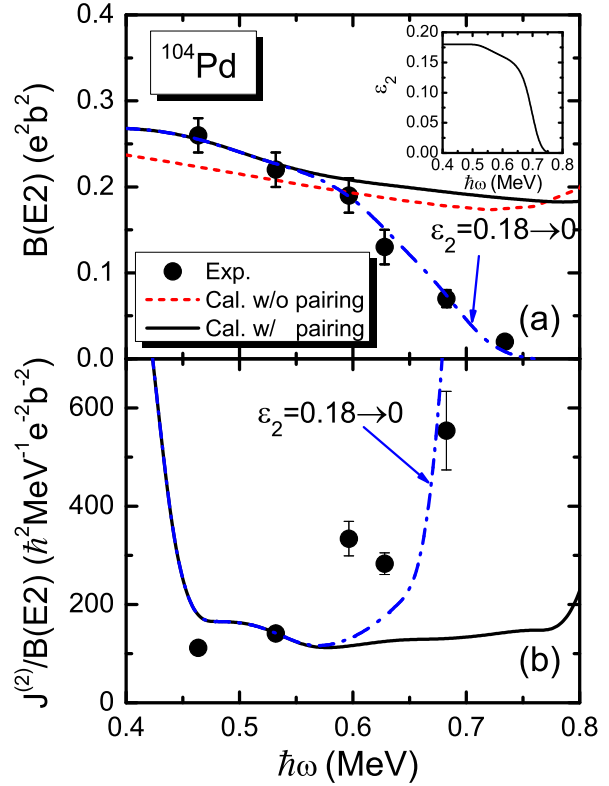


Fig. 3. (Color online) (a) The experimental [12] and calculated  $B(E2)$  values with and without pairing correlations for the gsb in  $^{104}\text{Pd}$ . (b) The comparison of experimental and calculated  $J^{(2)}/B(E2)$  ratios. The blue dash dotted line shows the calculated results with deformation  $\varepsilon_2$  changing from 0.18 to zero and the inset shows the deformation parameter  $\varepsilon_2$  adopted in this calculation.

Figure 4 shows the neutron and proton occupation probability  $n_\mu$  of each orbital  $\mu$  (including both  $\alpha = \pm 1/2$ ) near the Fermi surface of the gsb in  $^{104}\text{Pd}$ . It can be easily seen from Fig. 4(a) that at the rotational frequency  $\hbar\omega \sim 0.4$  MeV, the occupation probability for the neutron  $h_{11/2}$  orbital  $\nu 1/2^-[550]$  increases suddenly from about 0.4 to 2.0, while the occupation probabilities for some  $(g_{7/2}, d_{5/2})$  orbitals ( $\nu 3/2^+[411]$ ,  $\nu 5/2^+[413]$ , etc.) decrease. This indicates that the backbending may mainly be caused by the alignment of one pair of  $h_{11/2}$  neutron. Therefore, the AMR, in which the increase of angular momentum is caused by the contribution from proton, can happen in  $^{104}\text{Pd}$  only after the neutron level crossing. It also can be seen from Fig. 4(b) that at the similar rotational frequency, the occupation probability for the proton  $g_{9/2}$  orbital  $\pi 7/2^+[413]$  drops down from about 0.6 to about 0.1, while the occupation probabilities for other proton  $g_{9/2}$  orbitals, e.g.,  $\pi 5/2^+[422]$  and  $\pi 3/2^+[431]$ , increase gradually. The occupation rearrangements in proton  $g_{9/2}$  orbitals may also contribute

to the backbending, which is similar as  $^{101}\text{Pd}$  [33]. The present calculations show that after backbending, due to the existing of pairing correlations, the proton configuration of the AMR band is four partly empty proton  $g_{9/2}$  holes. As for the neutron, the configuration is two aligned  $h_{11/2}$  particles and about six particles in the  $(g_{7/2}, d_{5/2})$  orbitals. Note that the proton holes and neutron particles are written with respect to the  $^{100}\text{Sn}$  ( $N = 50$  and  $Z = 50$ ) core. When neglecting the pairing correlations, this configuration is consistent with that adopted in Ref. [26] by the TAC-CDFT. In addition, one can see from Fig. 4(b) that at the rotational frequency  $\hbar\omega \sim 0.8$  MeV, the occupation of  $\pi 1/2^+[431]$  increases from nearly zero to about 0.6, and the occupation of  $\pi 5/2^+[422]$  drops from 1.9 to 1.3. This is caused by the level crossing between these two orbitals due to the quick drop of  $\pi 1/2^+[431]$  with increasing rotational frequency, which can be easily seen from the cranked Nilsson levels in Fig. 1(a). This indicates that the AMR band observed in  $^{104}\text{Pd}$  will be terminated around this rotational frequency and a four quasiparticle band will appear, which is similar as that observed in  $^{143}\text{Eu}$  [13].

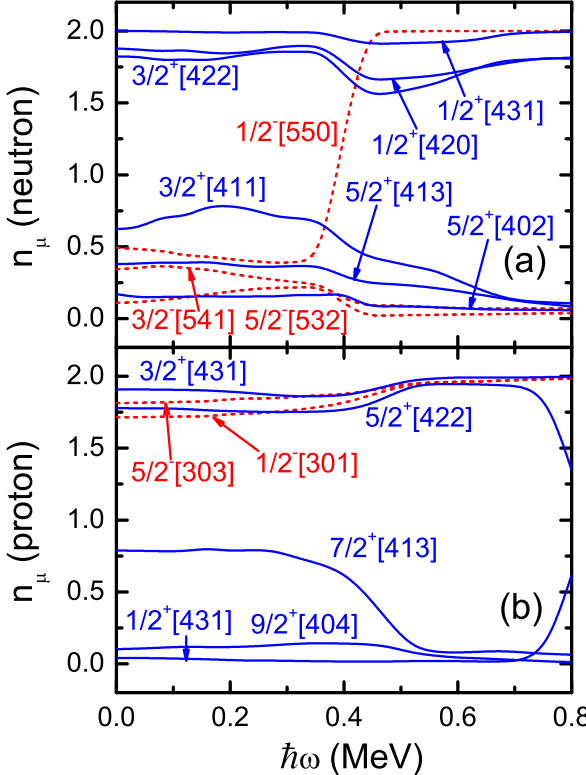


Fig. 4. (Color online) The neutron (a) and proton (b) occupation probability  $n_\mu$  of each orbital  $\mu$  (including both  $\alpha = \pm 1/2$ ) close to the Fermi surface of the gsb in  $^{104}\text{Pd}$ . The positive and negative parity levels are denoted by blue solid and red dashed lines. The Nilsson levels which are fully occupied ( $n_\mu \sim 0$ ) and fully empty ( $n_\mu \sim 2$ ) are not shown.

Figure 5 shows the experimental and calculated angular momentum alignment  $\langle J_x \rangle$  for the gsb in  $^{104}\text{Pd}$ . It can be seen from Fig. 5 that, there is a sharp increase of the neutron angular momentum alignment from rotational frequency  $\hbar\omega \sim 0.35$  MeV to about 0.45 MeV, which indicates again that this backbending mainly comes from the contribution of neutrons. Meanwhile, from  $\hbar\omega \sim 0.40$  MeV to about 0.55 MeV, the contribution from protons to  $\langle J_x \rangle$  also increases gradually. This increase comes from the rearrangement of proton occupations in  $g_{9/2}$  orbitals, which is similar as that in  $^{101}\text{Pd}$  [33]. It can be seen that before finishing the rearrangement of proton occupations in  $g_{9/2}$  orbitals between  $\hbar\omega \sim 0.45$  MeV to about 0.55 MeV, the contribution from the proton to  $\langle J_x \rangle$  is larger than the neutron. This indicates that the contribution from AMR to the increasing of  $\langle J_x \rangle$  is larger than that from the normal rotation. At  $\hbar\omega > 0.55$  MeV, the increase of neutron angular momentum alignment is faster than that of proton. This indicates that the contribution from AMR to the increasing of  $\langle J_x \rangle$  is smaller than that from the normal rotation. Therefore, the AMR in  $^{104}\text{Pd}$  may separate into two stages.

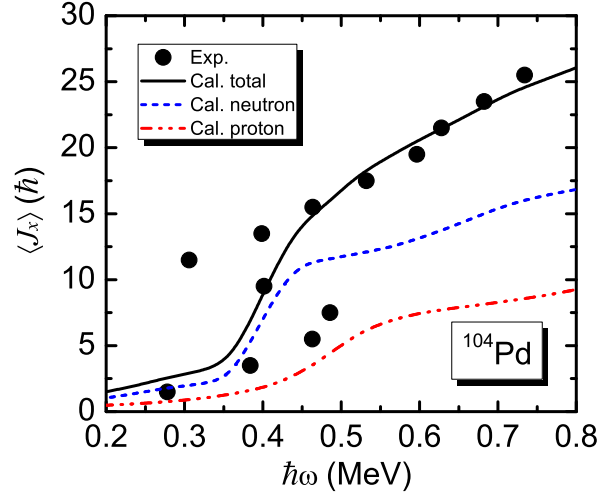


Fig. 5. (Color online) The experimental and calculated angular momentum alignment  $\langle J_x \rangle$  for the gsb in  $^{104}\text{Pd}$ .

To see the neutron and proton alignment process more clearly, the contributions of neutron and proton  $N = 4$  and 5 major shells to the angular momentum alignment  $\langle J_x \rangle$  for the gsb in  $^{104}\text{Pd}$  are shown in Fig. 6. The contributions of diagonal  $\sum_\mu j_x(\mu)$  and off-diagonal part  $\sum_{\mu<\nu} j_x(\mu\nu)$  in Eq. (6) from the neutron  $N = 5$  and proton  $N = 4$  major shell are denoted by dashed lines. It can be seen that the backbending around  $\hbar\omega \sim 0.4$  MeV mainly comes from the neutron  $N = 5$  major shell, especially from the diagonal part. Furthermore, if one looks into the details, the neutron diagonal part  $j_x(\nu 1/2^-[550])$  is mainly responsible for the backbending. In addition, the neutron  $N = 4$  major shell

provides a gradual increase of the angular momentum alignments after the neutron level crossing. This originates from the contribution of those neutron ( $g_{7/2}, d_{5/2}$ ) orbitals close to the Fermi surface. Fig. 6(b) shows that the proton  $N = 4$  major shell also contributes a gradual increase of the angular momentum alignment around the backbending frequency  $\hbar\omega \sim 0.4$  MeV, in which the off-diagonal part contributes a lot. Furthermore, the proton off-diagonal parts  $j_x(\pi 5/2^+[422]\pi 7/2^+[413])$ , and  $j_x(\pi 7/2^+[413]\pi 9/2^+[404])$  are mainly responsible for this gradual increase in proton angular momentum alignment. It also can be seen that at higher rotational frequency region with  $\hbar\omega > 0.55$  MeV, the increase of the angular momentum alignment from proton  $N = 4$  major shell is slower than that from the neutron  $N = 4$  major shell. This again tell us that the increase of the angular momentum alignment from AMR is less than that provided by the neutron ( $g_{7/2}, d_{5/2}$ ) orbitals at higher rotational frequency region.

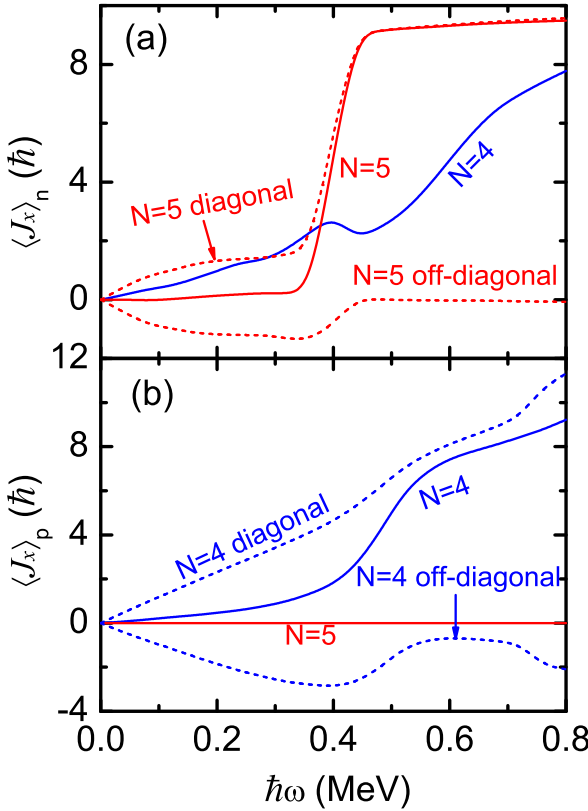


Fig. 6. (Color online) Contributions of (a) neutrons and (b) protons  $N = 4$  and 5 major shells to the angular momentum alignment  $\langle J_x \rangle$  for the gsb in  $^{104}\text{Pd}$ . Contributions of diagonal  $\sum_{\mu} j_x(\mu)$  and off-diagonal part  $\sum_{\mu < \nu} j_x(\mu\nu)$  (c.f., Eq. 6) from the neutron  $N = 5$  and proton  $N = 4$  major shells are denoted by dashed lines.

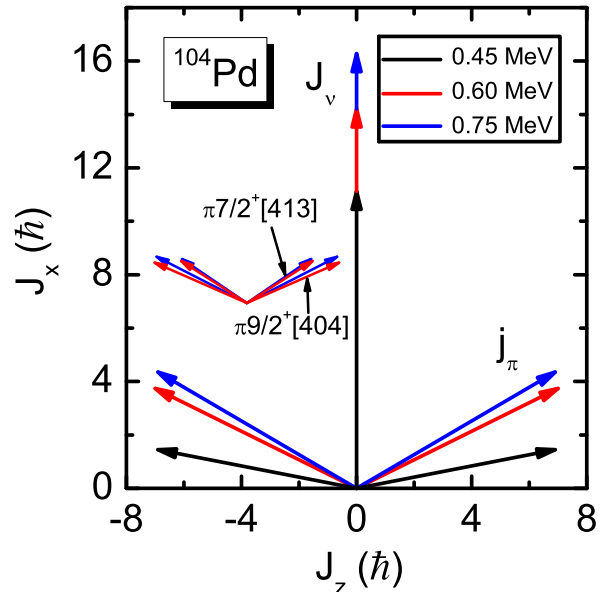


Fig. 7. (Color online) Angular momentum vectors of four proton  $g_{9/2}$  holes ( $j_{\pi}$ ) and neutrons ( $J_{\nu}$ ) for the gsb in  $^{104}\text{Pd}$ . Each  $j_{\pi}$  includes the contribution from two proton  $g_{9/2}$  holes. The inset shows the angular momentum vectors of four proton  $g_{9/2}$  holes ( $\pi 9/2^+[404]$  and  $\pi 7/2^+[413]$ ) separately by neglecting the off-diagonal part in Eq. 6.

Figure 7 shows the angular momentum vectors of four proton  $g_{9/2}$  holes ( $j_{\pi}$ ) and neutrons ( $J_{\nu}$ ) for the gsb in  $^{104}\text{Pd}$  at rotational frequencies from 0.45 to 0.75 MeV. Each  $j_{\pi}$  includes the contribution from two proton  $g_{9/2}$  holes. Note that due to the pairing correlations, the contribution from the off-diagonal part  $\sum_{\mu < \nu} j_x(\mu\nu)$  of protons is none zero (c.f., Fig. 6), especially at lower rotational frequency region ( $\hbar\omega=0.45$  to 0.60 MeV). Therefore, it is difficult to separate the contribution of each proton  $g_{9/2}$  hole to the angular momentum alignment to get the “umbrella”-like AMR mode as in Ref. [26]. However, with rotational frequency  $\hbar\omega > 0.60$  MeV, the four proton  $g_{9/2}$  holes are nearly empty and the contribution from the off-diagonal part to  $J_x$  becomes smaller. Therefore, we can separate the angular momenta of these four  $g_{9/2}$  holes approximately by neglecting the contribution from the off-diagonal part to  $J_x$ , which has been shown as an inset in Fig. 7. According to Ref. [45],  $J_z$  is calculated approximately by

$$J_z = \sqrt{\langle \Psi | J_z^2 | \Psi \rangle} \quad (13)$$

in the present PNC-CSM formalism. By comparing the principal axis cranking with the particle rotor model, this method has already been demonstrated to be a good approximation. One can see from Fig. 7 that at  $\hbar\omega = 0.45$  MeV, proton vectors  $j_{\pi}$  are pointing opposite direction and are nearly perpendicular to the neutron vector  $J_{\nu}$ . With rotational frequency increasing,

the two proton  $j_\pi$  vectors gradually close toward the neutron  $J_\nu$  vector, while the direction of the total angular momentum stays unchanged. Therefore, higher angular momentum is generated due to the “two-shears-like” mechanism. From rotational frequency  $\hbar\omega = 0.45$  to 0.75 MeV, the neutron angular momentum alignment increases smoothly. This is due to the alignment of neutrons in  $g_{7/2}$  and  $d_{5/2}$  orbitals, which is consistent with the TAC-CDFT calculations in Ref. [26]. The two proton blades close rapidly with rotational frequency  $\hbar\omega = 0.45$  to 0.60 MeV, and the magnitude of two  $j_\pi$  vectors keep no longer constant. This is similar as  $^{101}\text{Pd}$  [33], which originates from the occupation rearrangement in proton  $g_{9/2}$  orbitals. It should be noted that since pairing correlations are neglected in the TAC-CDFT calculations for  $^{104}\text{Pd}$  in Ref. [26], the four proton  $g_{9/2}$  holes are fully empty, and there is no proton occupation rearrangement process with increasing rotational frequency. Therefore, the proton blades with nearly constant magnitude close steadily with increasing rotational frequency, which is quite different from the angular momenta picture in the present PNC-CSM calculation. With rotational frequency increasing from 0.60 to 0.75 MeV, the close of two proton blades become slow and steady, which is similar with the typical AMR in  $^{105,106}\text{Cd}$  [32]. Therefore, two stages of AMR in  $^{104}\text{Pd}$  are clearly seen. It also can be seen from the inset of Fig. 7 that with the magnitude keeping constant, the angular momentum vectors of four proton  $g_{9/2}$  holes ( $\pi 9/2^+[404]$  and  $\pi 7/2^+[413]$ ) close

simultaneously with increasing rotational frequency. In addition, the two  $\pi 9/2^+[404]$  blades close more quickly than  $\pi 7/2^+[413]$  blades, which indicates that the two  $\pi 9/2^+[404]$  holes contribute more angular momenta in the typical AMR mode.

## 4 Summary

In summary, the particle-number-conserving method based on the cranked shell model is used to investigate the AMR band in  $^{104}\text{Pd}$ . The experimental MOIs are reproduced quite well. In order to reproduce the  $B(E2)$  values, a corresponding deformation change with increasing rotational frequency is necessary. The  $J^{(2)}/B(E2)$  ratios has also been discussed. The occupation probability of each orbital close to the Fermi surface and the contribution of each major shell to the total angular momentum alignment with rotational frequency are analyzed. The backbending mechanism of the ground state band in  $^{104}\text{Pd}$  is understood clearly and the configuration of the AMR after backbending is clarified. The present calculations suggest that the configuration of the AMR band in  $^{104}\text{Pd}$  should be  $\pi g_{9/2}^{-4} \otimes \nu [h_{11/2}^2, (g_{7/2}, d_{5/2})^6]$  when the pairing correlations are neglected, which is consistent with the TAC-CDFT calculations with PC-PK1. Furthermore, the crossing of a four quasiparticle states with this AMR band is also predicted. Finally, the “two-shears-like” mechanism for the AMR is investigated by examining the shears angle, and two stages of AMR in  $^{104}\text{Pd}$  are clearly seen.

## References

- 1 S. Frauendorf, in Proceedings of the Workshop on Gammasphere Physics, Berkeley, 1995, edited by M. A. Deleplanque, I. Y. Lee, and A. O. Macchiavelli (World Scientific, Singapore, 1996) p. 272.
- 2 S. Frauendorf, Rev. Mod. Phys. 73, 463 (2001).
- 3 D. Choudhury, A. K. Jain, M. Patial, N. Gupta, P. Arumugam, A. Dhal, R. K. Sinha, L. Chaturvedi, P. K. Joshi, T. Trivedi, R. Palit, S. Kumar, R. Garg, S. Mandal, D. Negi, G. Mohanto, S. Muralithar, R. P. Singh, N. Madhavan, R. K. Bhowmik, and S. C. Pancholi, Phys. Rev. C 82, 061308R (2010).
- 4 A. J. Simons, R. Wadsworth, D. G. Jenkins, R. M. Clark, M. Cromaz, M. A. Deleplanque, R. M. Diamond, P. Fallon, G. J. Lane, I. Y. Lee, A. O. Macchiavelli, F. S. Stephens, C. E. Svensson, K. Vetter, D. Ward, and S. Frauendorf, Phys. Rev. Lett. 91, 162501 (2003).
- 5 D. Choudhury, A. K. Jain, G. A. Kumar, S. Kumar, S. Singh, P. Singh, M. Sainath, T. Trivedi, J. Sethi, S. Saha, S. K. Jaddav, B. S. Naidu, R. Palit, H. C. Jain, L. Chaturvedi, and S. C. Pancholi, Phys. Rev. C 87, 034304 (2013).
- 6 A. J. Simons, R. Wadsworth, D. G. Jenkins, R. M. Clark, M. Cromaz, M. A. Deleplanque, R. M. Diamond, P. Fallon, G. J. Lane, I. Y. Lee, A. O. Macchiavelli, F. S. Stephens, C. E. Svensson, K. Vetter, D. Ward, S. Frauendorf, and Y. Gu, Phys. Rev. C 72, 024318 (2005).
- 7 P. Datta, S. Chattopadhyay, S. Bhattacharya, T. K. Ghosh, A. Goswami, S. Pal, M. S. Sarkar, H. C. Jain, P. K. Joshi, R. K. Bhowmik, R. Kumar, N. Madhavan, S. Muralithar, P. V. M. Rao, and R. P. Singh, Phys. Rev. C 71, 041305 (2005).
- 8 S. Roy, S. Chattopadhyay, P. Datta, S. Pal, S. Bhattacharya, R. Bhowmik, A. Goswami, H. Jain, R. Kumar, S. Muralithar, D. Negi, R. Palit, and R. Singh, Phys. Lett. B 694, 322 (2011).
- 9 M. Sugawara, T. Hayakawa, M. Oshima, Y. Toh, A. Osa, M. Matsuda, T. Shizuma, Y. Hatsukawa, H. Kusakari, T. Morikawa, Z. G. Gan, and T. Czosnyka, Phys. Rev. C 86, 034326 (2012).
- 10 M. Sugawara, T. Hayakawa, M. Oshima, Y. Toh, A. Osa, M. Matsuda, T. Shizuma, Y. Hatsukawa, H. Kusakari, T. Morikawa, Z. G. Gan, and T. Czosnyka, Phys. Rev. C 92, 024309 (2015).
- 11 V. Singh, S. Sihotra, S. Roy, M. Kaur, S. Saha, J. Sethi, R. Palit, N. Singh, S. S. Malik, H. C. Jain, and D. Mehta, J. Phys. G: Nucl. Part. Phys. 44, 075105 (2017).
- 12 N. Rather, S. Roy, P. Datta, S. Chattopadhyay, A. Goswami, S. Nag, R. Palit, S. Pal, S. Saha, J. Sethi, T. Trivedi, and H. C. Jain, Phys. Rev. C 89, 061303R (2014).
- 13 S. Rajbanshi, S. Roy, S. Nag, A. Bisoi, S. Saha, J. Sethi, T. Bhattacharjee, S. Bhattacharyya, S. Chattopadhyay, G. Gangopadhyay, G. Mukherjee, R. Palit, R. Raut, M. S. Sarkar, A. Singh, T. Trivedi, and A. Goswami, Phys. Lett. B 748, 387 (2015).
- 14 S. Ali, S. Rajbanshi, B. Das, S. Chattopadhyay, M. Saha Sarkar, A. Goswami, R. Raut, A. Bisoi, S. Nag, S. Saha, J.

---

Sethi, R. Palit, G. Gangopadhyay, T. Bhattacharjee, S. Bhattacharyya, G. Mukherjee, A. K. Singh, and T. Trivedi, Phys. Rev. C 96, 021304 (2017).

15 C. J. Chiara, S. J. Asztalos, B. Busse, R. M. Clark, M. Cromaz, M. A. Deleplanque, R. M. Diamond, P. Fallon, D. B. Fossan, D. G. Jenkins, S. Juutinen, N. S. Kelsall, R. Krücken, G. J. Lane, I. Y. Lee, A. O. Macchiavelli, R. W. MacLeod, G. Schmid, J. M. Sears, J. F. Smith, F. S. Stephens, K. Vetter, R. Wadsworth, and S. Frauendorf, Phys. Rev. C 61, 034318 (2000).

16 S. Zhu, U. Garg, A. V. Afanasjev, S. Frauendorf, B. Kharraja, S. S. Ghugre, S. N. Chintalapudi, R. V. F. Janssens, M. P. Carpenter, F. G. Kondev, and T. Lauritsen, Phys. Rev. C 64, 041302R (2001).

17 M. Sugawara, Y. Toh, M. Oshima, M. Koizumi, A. Osa, A. Kimura, Y. Hatsukawa, J. Goto, H. Kusakari, T. Morikawa, Y. H. Zhang, X. H. Zhou, Y. X. Guo, and M. L. Liu, Phys. Rev. C 79, 064321 (2009).

18 X. W. Li, J. Li, J. B. Lu, K. Y. Ma, Y. H. Wu, L. H. Zhu, C. Y. He, X. Q. Li, Y. Zheng, G. S. Li, X. G. Wu, Y. J. Ma, and Y. Z. Liu, Phys. Rev. C 86, 057305 (2012).

19 R. M. Clark and A. O. Macchiavelli, Annu. Rev. Nucl. Part. Sci. 50, 1 (2000).

20 S. Frauendorf, Nucl. Phys. A 677, 115 (2000).

21 J. Peng, J. Meng, P. Ring, and S. Q. Zhang, Phys. Rev. C 78, 024313 (2008).

22 P. W. Zhao, S. Q. Zhang, J. Peng, H. Z. Liang, P. Ring, and J. Meng, Phys. Lett. B 699, 181 (2011).

23 P. W. Zhao, J. Peng, H. Z. Liang, P. Ring, and J. Meng, Phys. Rev. Lett. 107, 122501 (2011).

24 P. W. Zhao, J. Peng, H. Z. Liang, P. Ring, and J. Meng, Phys. Rev. C 85, 054310 (2012).

25 J. Peng and P. W. Zhao, Phys. Rev. C 91, 044329 (2015).

26 H. Jia, B. Qi, C. Liu, Q. Hu, and S. Y. Wang, Phys. Rev. C 97, 024335 (2018).

27 J. Meng, J. Peng, S. Q. Zhang, and P. W. Zhao, Front. Phys. 8, 55 (2013).

28 P. W. Zhao, and Z. P. Li, Int. J. Mod. Phys. E 27, 1830007 (2018).

29 P. W. Zhao, Z. P. Li, J. M. Yao, and J. Meng, Phys. Rev. C 82, 054319 (2010).

30 J. Y. Zeng and T. S. Cheng, Nucl. Phys. A 405, 1 (1983).

31 J. Y. Zeng, T. H. Jin, and Z. J. Zhao, Phys. Rev. C 50, 1388 (1994).

32 Z.-H. Zhang, P.-W. Zhao, J. Meng, J.-Y. Zeng, E.-G. Zhao, and S.-G. Zhou, Phys. Rev. C 87, 054314 (2013).

33 Z.-H. Zhang, Phys. Rev. C 94, 034305 (2016).

34 C. S. Wu and J. Y. Zeng, Phys. Rev. C 39, 666 (1989).

35 J. Meng, J.-Y. Guo, L. Liu, and S.-Q. Zhang, Front. Phys. China 1, 38 (2006).

36 Z. Shi, Z. H. Zhang, Q. B. Chen, S. Q. Zhang, and J. Meng, Phys. Rev. C 97, 034317 (2018).

37 N. Pillet, P. Quentin, and J. Libert, Nucl. Phys. A 697, 141 (2002).

38 W. Y. Liang, C. F. Jiao, Q. Wu, X. M. Fu, and F. R. Xu, Phys. Rev. C 92, 064325 (2015).

39 X. M. Fu, F. R. Xu, J. C. Pei, C. F. Jiao, Y. Shi, Z. H. Zhang, and Y. A. Lei, Phys. Rev. C 87, 044319 (2013).

40 S. G. Nilsson, C. F. Tsang, A. Sobiczewski, Z. Szymański, S. Wycech, C. Gustafson, I.-L. Lamm, P. Möller, and B. Nilsson, Nucl. Phys. A 131, 1 (1969).

41 H. Molique and J. Dudek, Phys. Rev. C 56, 1795 (1997).

42 T. Bengtsson and I. Ragnarsson, Nucl. Phys. A 436, 14 (1985).

43 I. Hamamoto, Nucl. Phys. A 271, 15 (1976).

44 S. Ćwiok, J. Dudek, and Z. Szymański, Phys. Lett. B 76, 263 (1978).

45 S. Frauendorf and J. Meng, Z. Phys. A 356, 263 (1996).